

Accepted Manuscript



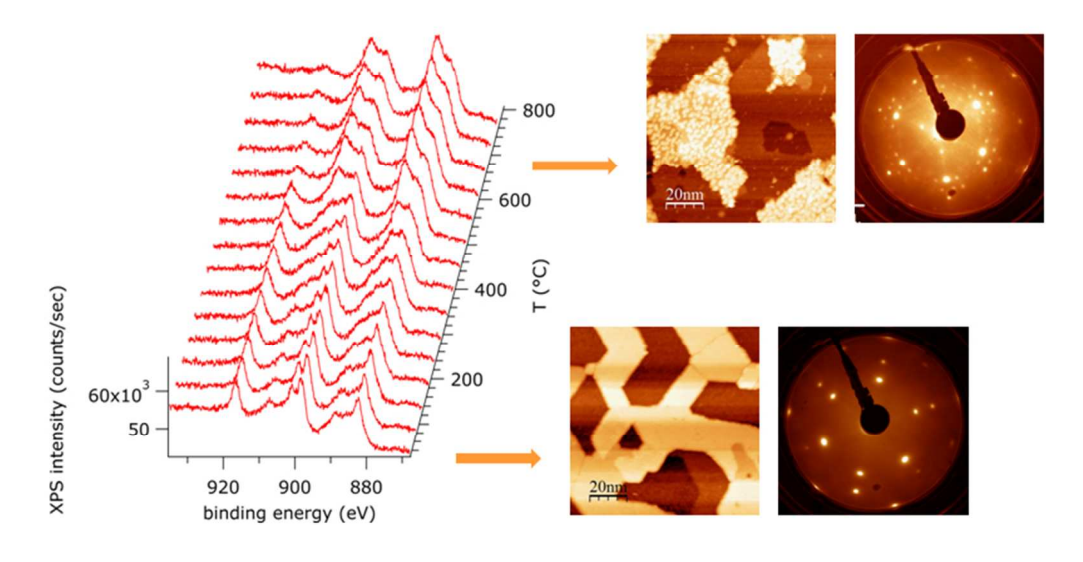
This is an *Accepted Manuscript*, which has been through the Royal Society of Chemistry peer review process and has been accepted for publication.

Accepted Manuscripts are published online shortly after acceptance, before technical editing, formatting and proof reading. Using this free service, authors can make their results available to the community, in citable form, before we publish the edited article. We will replace this Accepted Manuscript with the edited and formatted Advance Article as soon as it is available.

You can find more information about *Accepted Manuscripts* in the **Information for Authors**.

Please note that technical editing may introduce minor changes to the text and/or graphics, which may alter content. The journal's standard <u>Terms & Conditions</u> and the <u>Ethical guidelines</u> still apply. In no event shall the Royal Society of Chemistry be held responsible for any errors or omissions in this *Accepted Manuscript* or any consequences arising from the use of any information it contains.





Thermal treatments in vacuum and oxygen induce reversible modifications in stoichiometry, surface morphology and structure of epitaxial CeO2 films.

281x152mm (72 x 72 DPI)

Journal Name

RSCPublishing

ARTICLE

Cite this: DOI: 10.1039/x0xx00000x

Received ooth January 2012, Accepted ooth January 2012

DOI: 10.1039/x0xx00000x

www.rsc.org/

Structural and morphological modifications in thermally reduced cerium oxide ultrathin epitaxial films on Pt(111)

P. Luches^a, F. Pagliuca^{a,b}, S. Valeri^{a,b}

The modifications of stoichiometry, morphology and surface structure of cerium oxide ultrathin films induced by thermal treatments in vacuum and in oxygen partial pressure were studied using *in-situ* X-ray photoemission spectroscopy, scanning tunnelling microscopy and low energy electron diffraction. The effect of the film nominal thickness, heating temperature and heating time on the degree of reduction of the film were investigated. The reduction is more relevant on the film surface, where different ordered surface structures were observed at different degrees of reduction for very thin films. The obtained results are discussed taking into account the dimensionality of the oxide and the effects of the proximity of the Pt substrate. After reduction it was always possible to re-oxidize the films back to their original oxidation state by thermal treatments in oxygen-rich conditions.

1 Introduction

Reducible oxides are materials in which the cation oxidation state can be reversibly changed between two or more states. This property is connected with the facility for the material to form and fill oxygen vacancies depending on the ambient conditions, and gives origin to the so called oxygen storage capacity. The reducibility of cerium oxide makes this material very appealing for a number of applications, in particular in catalysis¹, fuel cells² and biomedicine.³

The control and optimization of the reducibility in oxides is a challenging task, which requires a fundamental understanding of the electronic properties and of their modifications induced for example by spatial confinement, morphology, proximity with other atomic species in the substrate, in supported nanoparticles or as dopants. The study of reduction processes in epitaxial films with well controlled single crystalline surfaces allows to simultaneously determine electronic, morphological and structural changes by means of surface science techniques and to compare them with the results of theoretical models. Cerium oxide films with the fluorite structure and a (111) surface orientation have been shown to grow epitaxially on Pt(111)⁶⁻¹⁰ and on a number of different metallic 11-13 and semiconducting surfaces. The films, in general, show atomically flat terraces with straight edges, similar to the ones

shown by single crystal (111) surfaces. 16 Ceria surfaces with low concentration of oxygen vacancies have been obtained either by heating in vacuum^{4,11,17,18} or by mild electron sputtering⁵ and investigated to determine the mechanisms responsible for oxygen vacancy formation in single crystalline systems. The debates on the relative stability of surface and subsurface oxygen vacancies and on the degree of localization of the electronic charge left by oxygen atoms removed from the lattice are ongoing.^{4,5,19-21} High-temperature heating treatments in ultra-high vacuum have shown to induce a significant reduction in cerium oxide films. 10,11,15,22 Heavily reduced surfaces have been prepared also by thermal treatments in reducing gases such as hydrogen,²³ ethanol²⁴ or methanol,²⁵ by Ar⁺ bombardment^{23,26} and by reactive deposition of metallic Ce in low oxygen partial pressure. 27-29 Recently, a Ce₇O₁₂ surface phase has been stabilized on reduced thick ceria films.³⁰ At higher reduction degrees a number of experiments report the formation of the hexagonal a-Ce2O3 structure8,27,31 while the cubic bixbiyte structure has been demonstrated to be stabilized in a few recent studies on Si(111)³² and on Cu(111)³³ under specific experimental conditions, in the latter case by interfacial reaction between cerium dioxide and metallic cerium.

In general, the mechanisms responsible for reduction, for the modification of the structure and for the stabilization of a specific reduced phase strongly depend on the experimental procedure and on the specific system studied, and a thorough understanding of the mechanisms which take place requires further investigation.

This work is focussed on the study of reversible reduction processes of cerium oxide films grown on a Pt(111) surface. The reduction/oxidation is induced by thermal treatments in

^a Istituto Nanoscienze - CNR, Via G. Campi 213/a, 41125 Modena, Italy

Dipartimento di Scienze Fisiche Informatiche e Matematiche, Via
G. Campi 213/a, 41125 Modena, Italy

ultra-high vacuum (UHV) and oxygen-rich atmosphere and studied by *in-situ* X-ray photoemission spectroscopy (XPS), low-energy electron diffraction (LEED) and scanning tunneling microscopy (STM). The investigation has been performed for different film thickness, heating times, heating rates and temperatures and provides a complete picture of the processes taking place in this specific system.

The results allow to understand the behavior of a model system for catalytically active materials, such as the ceria/Pt system, and they are of help to improve the understanding of reducibility in ceria/metal systems.

2. Experimental apparatus and procedures

The samples used for the present study have been prepared in an ultra-high vacuum (UHV) chamber (base pressure 1×10⁻¹⁰ Torr), equipped with facilities for substrate preparation, film growth and for in-situ XPS, LEED, and STM analysis. The substrate used was a Pt(111) single crystal surface prepared by repeated cycles of sputtering (1 KeV, 1 µA) and annealing (1040 K), until the concentration of surface contaminants was below the XPS detection level and the LEED showed sharp spots with hexagonal symmetry. The films were prepared by evaporating Ce from an electron bombardment evaporation cell in oxygen partial pressure $(P_{O2}=1\times10^{-7} \text{ mbar})$, keeping the substrate at room temperature (RT). The cell was calibrated by a quartz crystal microbalance to give a Ce evaporation rate of ~ 0.2 Å/min. To optimize surface flatness, film stoichiometry and structural long range order, the films were annealed at 770°C in P_{O2}=1×10⁻⁷ mbar for 15 min after growth, following the results of a previous work. 10 The ceria film thickness is given in terms of deposited monolayer (ML), where 1 ML corresponds to the thickness of one O-Ce-O trilayer, i.e. 3.12 Å. Reducing thermal treatments were performed using an electron bombardment heater. The sample temperatures were measured by a thermocouple in contact with the sample holder very close to the sample position and are assumed to be accurate within approximately $\pm 10^{\circ}$. To investigate also the time dependence of the reduction process, the heating rate was modified between 20°C/min, referred in the following as the slow heating mode, and a fast heating mode, in which the heating rate was as fast as possible for the sample heater and power supplies of the available setup, i.e. 180°C/min up to 500°C, 120°C/min up to 700°C, 60°C/min up to 750°C and 30°C/min up to 770°C. The cooling was also performed in a slow cooling mode (20°C/min) or in a fast cooling mode (180°C/min). The oxidizing thermal treatments were performed using the same heating ramps, in an oxygen partial pressure of P_{O2} in the range 2×10^{-8} - 1×10^{-7} mbar.

XPS measurements were performed using a non monochromatic Al K_{α} X-ray source (1486.6 eV) and a hemispherical electron analyzer. The intensities of Pt 4f and Ce 3d XPS spectra were evaluated by measuring the area of the peaks after the removal of a Shirley-type background. The Ce 3d XPS spectra were also fit to obtain the relative weight of the contribution given by Ce^{3+} and Ce^{4+} ions. Following the procedures exposed in references 34 and 35 the fitting was performed using five doublets and a Shirley-type background, with the area of the doublets as the only fitting parameter. The absolute values of the ionic concentration obtained in this way are not very accurate, since the origin of the spectral features has not been fully and unambiguously assigned. 34,36,37 However, most of the considerations made in the following are based on the relative modifications of the ionic concentrations in the different samples/conditions.

The STM was operated at RT in constant current mode, using electrochemically etched tungsten tips, degassed by thermal treatments and sputtered by ion bombardment before the measurements. The STM images have been processed using the WSXM software.³⁸

To compare the reducibility of films with different nominal thickness two samples, 2 and 10 ML thick, were treated by thermal cycles as follows: heating to 770°C in UHV and keeping the sample for 15 min at 770°C; cooling to RT in UHV. The same heating and cooling treatment was repeated in $P_{\rm O2}$ =2×10⁻⁸ mbar. During the thermal cycles the samples were monitored by XPS following the evolution of Ce 3d spectra, while at the end of each heating/cooling branch also the Pt 4f and O 1s XPS spectra were acquired. After the thermal treatment in UHV and in O_2 the samples were characterized also by LEED and STM. Other samples of different thickness, treated by different thermal cycles and different heating modes, have also been studied to clarify specific issues, e.g. the dependence of reduction on heating time, the depth distribution of reduced species and the origin of the morphological features related to reduction.

3. Results

3.1 XPS

The aim of this study is to determine the factors which influence reducibility in ultrathin cerium oxide films on Pt. The degree of reduction of the different samples investigated was determined by the analysis of Ce 3d XPS spectra. To reliably compare the Ce³⁺ concentration measured by XPS in different samples, the first issue investigated is the dependence of the measured Ce³⁺ concentration on heating time in UHV. Fig.1 b shows the Ce 3d spectra of a 3 ML cerium oxide sample heated at 770°C using in the fast heating mode at different heating times. The evolution of the shape of the spectra clearly indicates a progressive reduction of the films with heating time:

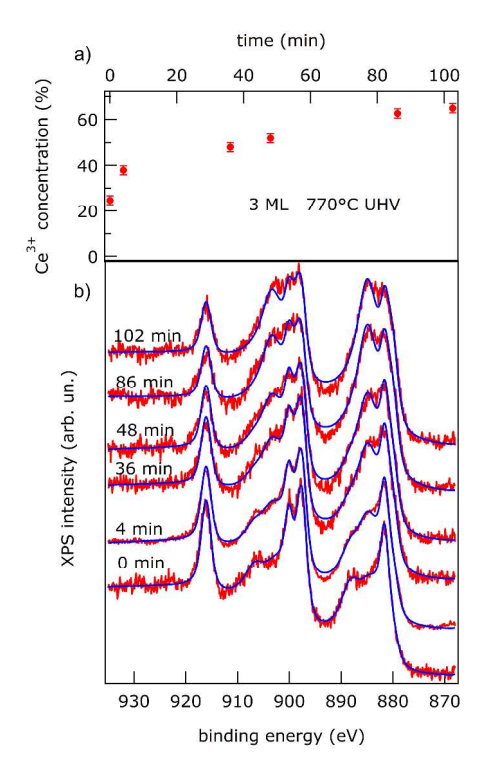


Fig. 1: (a) Ce^{3+} concentration and (b) Ce 3d XPS spectra (red) and fits (blue) measured on a 3 ML cerium oxide film measured while heating the sample at 770°C in UHV for different times.

the Ce⁴⁺ - related feature at 916.5 eV decreases in intensity and the shapes of the other two main spectral features at lower binding energy also change significantly. The values of the measured Ce³⁺ concentration obtained by fitting of the spectra as a function of time are reported in Fig.1a. A relevant increase of the measured Ce³⁺ concentration from 25% to 65% is observed as a function of time within 100 min at 770° C (Fig.1a). This evidence indicates that, if the heating is fast enough, the density of oxygen vacancies formed during the heating do not reach an equilibrium value. This is probably due to the limited mobility of oxygen ions at the considered temperature. In the comparison of the degree of reduction of different samples, therefore, care has to be taken in using the same heating cycles, not only in terms of final temperatures but also of heating rates and duration of the heating at a specific temperature. A dependence of the final degree of reduction on the cooling rate was observed also on thick cerium oxide films on Si(111).15

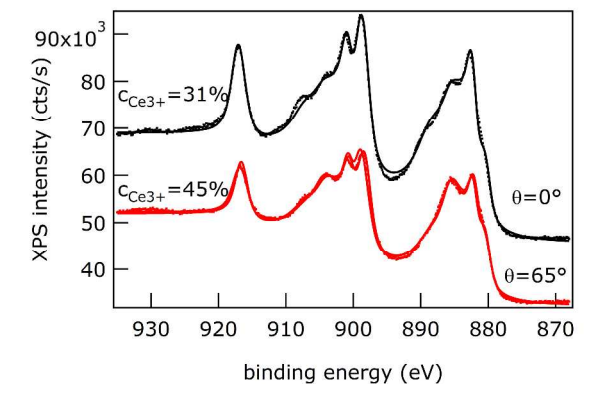


Fig. 2: Ce 3d XPS spectra of a 5 ML cerium oxide film after UHV heating at 770°C for 15 min measured at 0° (black dots) and 65° (red dots) take-off angles. The fits are also shown as a solid line.

In order to have information on the depth localization of reduced species, angle resolved XPS measurements were acquired. Fig.2 shows the Ce 3d XPS spectra and the corresponding fits for a 5 ML cerium oxide film after UHV heating at 770°C for 15 min and cooling to RT in the fast heating/cooling mode at take-off angles of 0° and 65° from sample normal. We note that the Ce³⁺ concentration measured at grazing take-off angles (c_{Ce3+} =45%) is larger than the one measured at normal emission (c_{Ce3+} =31%), confirming that the Ce reduction is more relevant on the sample surface. A quantitative evaluation of the absolute amount of Ce³⁺ in the samples is hindered by the fact that the Ce³⁺ concentration is expected to evolve from a minimum value in the bulk to a maximum value on the surface, which depends on temperature and heating time, with an unknown profile.

To investigate the dependence of reducibility on the film thickness, we investigated the modifications induced in Ce 3d spectra by thermal treatments in vacuum and in oxygen partial pressure in two samples, 2 and 10 ML thick. Fig.3a shows Ce 3d XPS spectra for the 2 ML cerium oxide film acquired during sample heating in UHV up to 770°C in the slow heating mode. The evolution of the shape of the spectra with T clearly shows that the sample is reduced during UHV heating. The area of the Ce 3d peak is not relevantly modified by the heating, allowing to exclude any significant CePt alloy formation. Similar series of Ce 3d spectra (not shown) have been acquired also during sample cooling and during the thermal cycle in O2. To obtain a quantitative evaluation of the evolution of the Ce³ concentration, we fitted each spectrum of the full heating cycles in vacuum and in oxygen. An example of the fit quality is reported in Fig.3b, which also shows the different components used: three doublets originating from Ce4+ ions and two doublets from Ce3+ ions. The results of the fitting of the full thermal cycle, in vacuum and in oxygen, for the 2 ML sample are shown in Fig.3c. The Ce initial oxidation state of the 2 ML sample is not fully 4+, as already observed for low dimensional cerium oxide features on Pt(111),10 due to the high concentration of low coordination sites and to a possible charge transfer from the substrate.³⁹ Further sample reduction starts around 200°C, and it reaches a saturation level corresponding to a measured Ce³⁺ concentration of 80%. The Ce³⁺ concentration decreases only slightly after cooling in UHV and after heating in O₂ partial pressure up to 500°C. The sample starts being reoxidized significantly only after heating in O₂ above 500°C. Cooling in O₂ is necessary to bring the sample oxidation state back to the original one. After the full cycle the ratio between the intensity of Ce 3d and Pt 4f XPS is decreased from 0.93 to 0.76, suggesting that some modifications in morphology have occurred after the thermal treatment. This effect has been investigated by STM and it will be discussed in subsection 3.2. The same heating cycle in UHV and in oxygen partial pressure was performed on a 10 ML thick cerium oxide film. The results of the fitting of Ce 3d XPS spectra measured during the cycles are reported in Fig.3d. At variance with the 2 ML sample, for the 10 ML film the measured Ce³⁺ concentration starts to increase only around 450°C and it reaches a saturation level of approximately 50% above 600°C. Also in this case the reoxidation after cooling at RT in UHV is not very relevant and a heating treatment in O_2 is necessary to re-oxidize the sample. The reversibility of the reduction process, demonstrated for the cerium oxide films of different thickness is a very relevant issue, which must be checked whenever dealing with the reducibility of an oxide. In fact it was shown that some Cebased oxides, like for example cerium silicates, do not show this interesting property on which the applications are based. 40 For the 10 ML sample, after the full thermal cycle, the ratio between the intensity of Ce 3d and Pt 4f XPS is unaltered (I_{Ce}/I_{Pt}=6.3), suggesting negligible long range modification of the morphology after the thermal treatments.

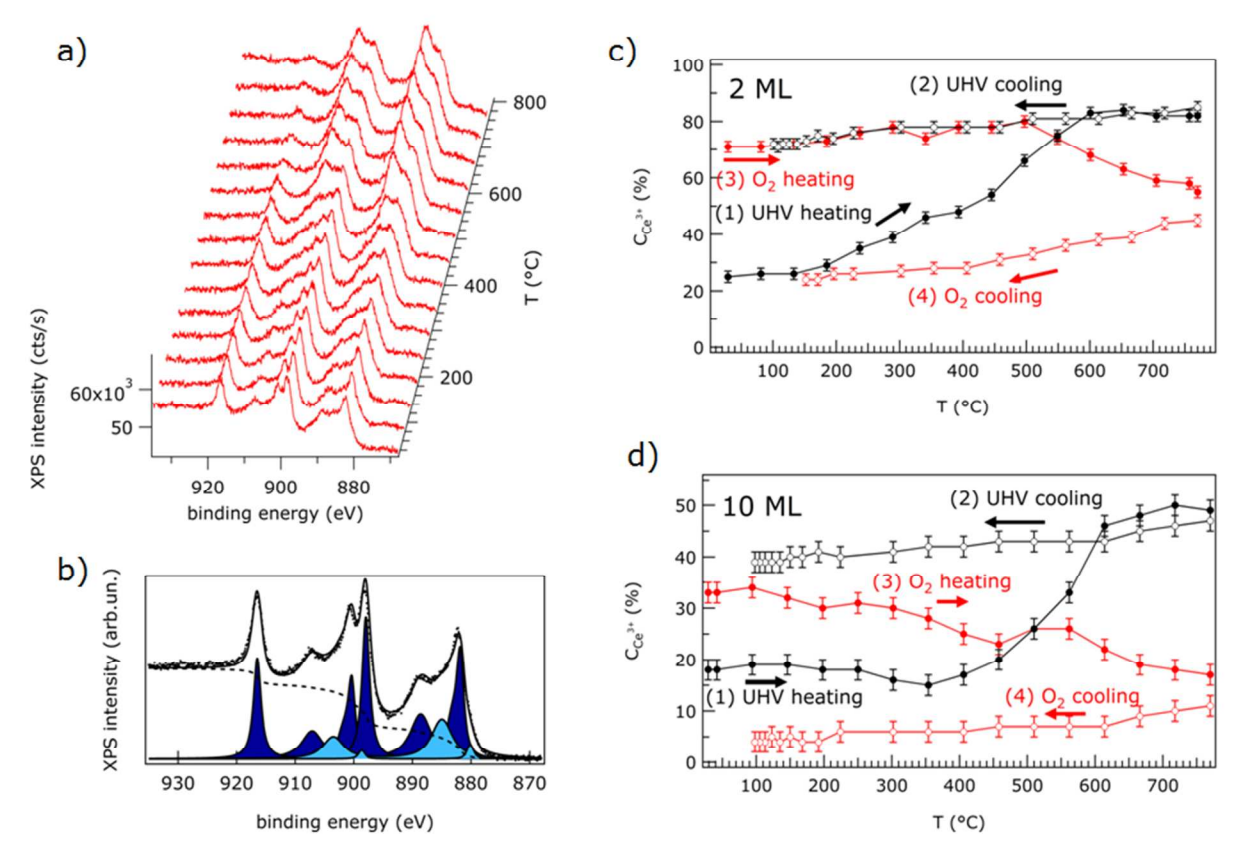


Fig. 3: a) Ce 3d XPS spectra for a 2 ML cerium oxide film measured at increasing heating temperature in UHV; b) Ce 3d XPS spectrum of a 2 ML film as prepared (dots), fit (solid line), Shirley type background (dashed line) and components ascribed to Ce^{3+} (light blue) and Ce^{4+} (dark blue) ions; c) Ce^{3+} concentration obtained by fitting the Ce 3d XPS spectra of a 2 ML thick film during thermal cycles in UHV and in O_2 partial pressure; d) Ce^{3+} concentration obtained by fitting the Ce 3d XPS spectra of a 10 ML thick film during thermal cycles in UHV and in O_2 partial pressure.

3.2 STM

The morphology of the films and its evolution with the thermal treatments was studied by STM. The full details of the film morphology of cerium oxide films of different thickness, grown in the same conditions used for this study, have already been discussed in a previous work. 10 As shown in Fig. 4a, after the deposition of a nominal oxide thickness of 2 ML, cerium oxide forms islands covering approximately 50% of the Pt surface. The islands have atomically flat surfaces and straight borders mainly forming angles of 120°, i.e. aligned along the surface [110] directions. The height of the cerium oxide islands ranges between 2 and 3 ML. Considering the average island height and the surface coverage measured on several images, the actual amount of cerium oxide deposited results a bit less than 2 ML. This is probably due to some degree of instability of the Ce evaporation cell. After the heating treatment in UHV at 770°C and the subsequent cooling at RT the long range morphology of the 2 ML sample changed (Fig.4b). In particular the Pt surface coverage decreased to approximately 30% and the cerium oxide islands height increased to up to 4 ML in some areas. This modification accounts for the decrease in Ce 3d/Pt 4f XPS intensity ratio observed after reduction (sect. 3.1). Furthermore,

the islands surface appears corrugated, hindering the possibility of acquiring images at a high resolution. After sample reoxidation by heating in oxygen partial pressure at 770°C for 15 min the morphology of the cerium oxide islands shows a further change, as shown in Fig.4c, with some additional features appearing. The additional features are rather high (up to 4-5 nm) and tend to show a rectangular shape. Further investigation is needed to clarify their origin, which goes beyond the scope of this work.

The 10 ML thick film shows a surface exposing different cerium oxide (111) layers, with extended holes and linear defects (Fig.4d). The maximum measured depth of the holes is 2 nm and their width ranges up to 10 nm. On the uppermost ceria plane some topographic features with rather straight borders forming mainly 120° angles can be observed. Their lateral size ranges from a few nm to 25 nm approximately and they protrude from the uppermost ceria layer by 3.1 Å, i.e. one CeO₂ ML. After heating and cooling in UHV the sample long range morphology showed some modifications (Fig.4e): the small ceria features on the surface disappeared and a number of much smaller apparent protrusions are evident on the surface. These features appear a few nm wide and a few Å high. As shown in Fig.4f, after annealing in oxygen partial pressure, the small features disappear, suggesting that their presence is connected with reduction.

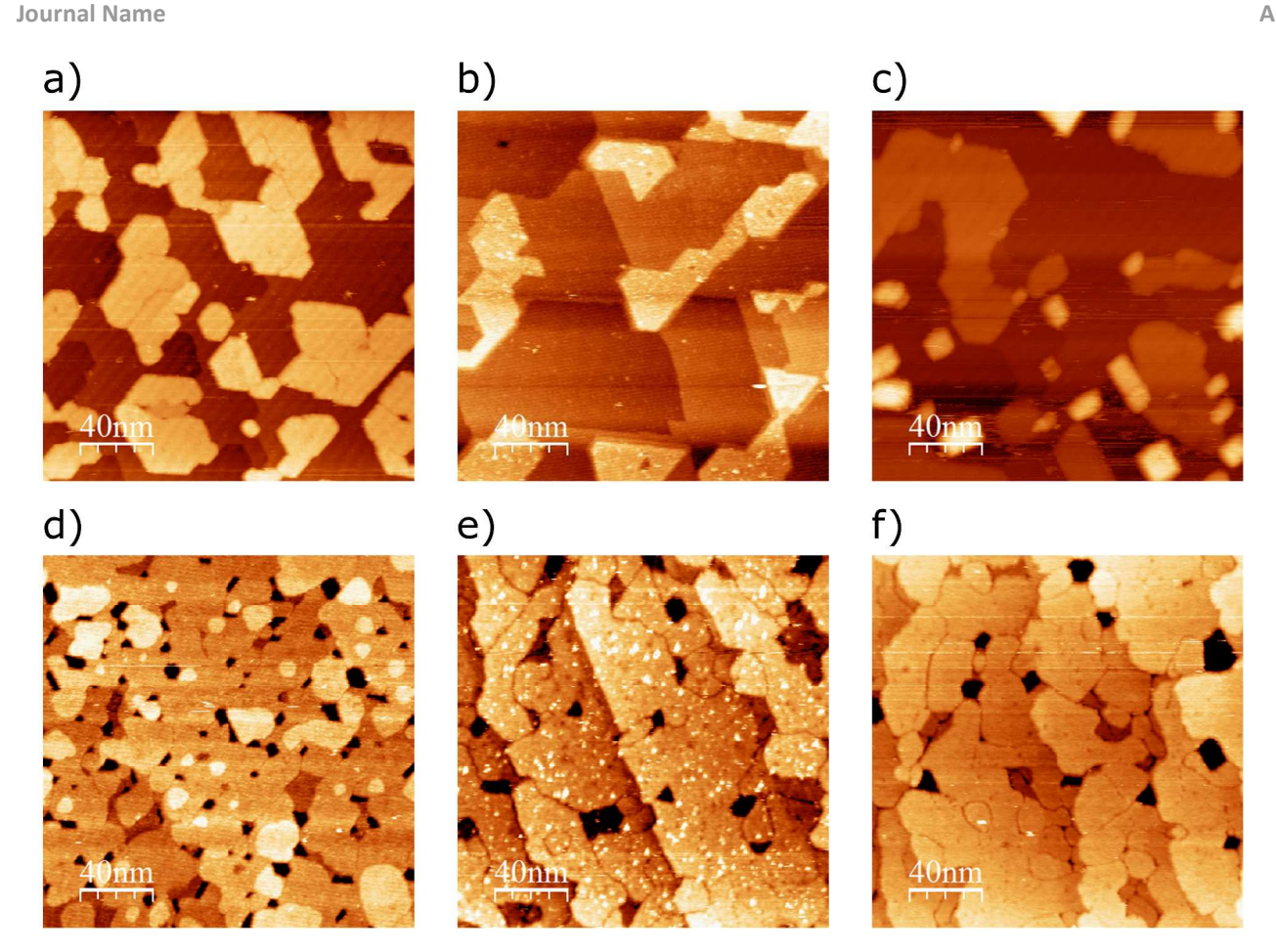


Fig. 4: STM images of a 2 ML sample a) as prepared (I=0.08 nA V=1.6 V), b) after UHV heating at 770° C (I=0.08 nA V=1 V), c) after heating at 770° C in O_2 (I=0.08 nA V=2 V) and of a 10 ML sample d) as prepared (I=0.1 nA V=3 V), e) after UHV heating at 770° C (I=0.1 nA V=2 V), f) after heating at 770° C in O_2 (I=0.1 nA V=3 V).

In order to get more information on the reduction-related changes in morphology, we investigated by STM a further set of samples, with nominally the same thickness as the previous ones (2 and 10 ML), which were processed by different thermal treatments, i.e. by heating at lower temperatures for longer times. In this way, we expected to minimize large scale morphological modifications and to be able to isolate reductioninduced morphological modifications. Fig.5a shows the topography of a 2 ML sample before reduction. Similar considerations as the ones made for the 2 ML sample of Fig.4a hold, although the coverage appears slightly higher. Fig.5b shows the evolution of the surface morphology after heating at 500°C in UHV for 165 min. The most evident change are some apparent protrusions on the sample surface. The observed features have lateral size and height similar to the features observed on the 10 ML sample after reduction (Fig.4e), a diameter of a few nm and a height of a few Å, and they cover a large fraction of the surface of cerium oxide islands.

Furthermore, a slight overall modification in the long range morphology can be observed, with the islands being more disconnected than before the annealing. The XPS indicated a Ce³⁺ concentration of 63% after the treatment. After reoxidation by heating in $P_{O_2}=1\times10^{-7}$ mbar at 500°C for 1 hour (Fig.5c), which brings the oxidation state as measured by XPS back to the original one after preparation, the long range morphology is rather different from the original one. The cerium oxide islands are 3-4 ML thick in their inner parts, while a 2 ML thick region extends at the edge between the islands and uncovered Pt areas. The clusters disappeared from the oxide film surface after reoxidation as shown by the inset of Fig.5c. Some 1-2 nm features up to 2 nm high and a few nm in lateral size protrude from the Pt surface and they possibly have the same origin as the ones observed on the 2 ML film after heating in O₂ at 770°C (Fig.4c), although they are smaller in size.

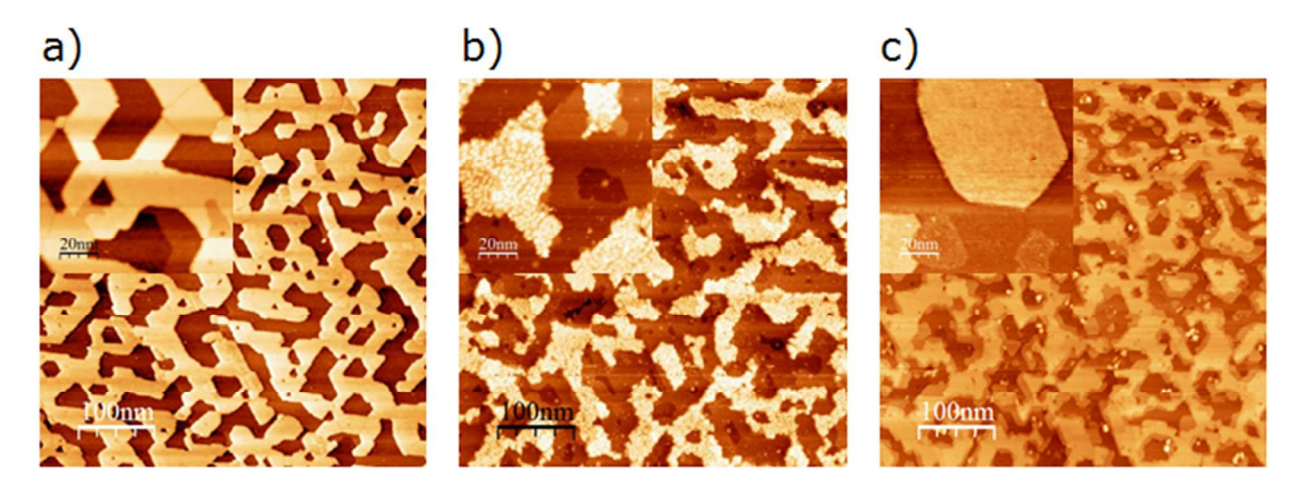


Fig. 5: STM images of a 2 ML sample a) as prepared (I=0.2 nA V=18 V; inset I=0.2 nA V=2 V), b) after UHV heating to 500°C for 165 min (I=0.2 nA V=2 V; inset I=0.1 nA V=1.8 V), e) after heating to 500°C in O₂ for 1 hour (I=0.2 nA V=2 V; inset I=0.39 nA V= 1.5 V).

In Fig.6a and b we show the STM images of a 10 ML film before and after heating in UHV at 500°C for 165 min. At variance with the case of the 2 ML film, where this thermal treatment brought a very relevant modification in morphology (Fig.5b), the 10 ML sample did not show evident modifications of the surface. A temperature of 500°C lies within the range in which reduction is negligible on 10 ML films and significant in 2 ML films (See Fig.3c and d). Consistently, the fitting of the Ce 3d XPS spectrum (not shown) gives a Ce³⁺ concentration of 4% for this sample, consistent with the absence of relevant

Fig. 6: STM images of a 10 ML sample a) as prepared (I=0.1 nA V=3.8 V); b) after UHV heating to 500° C for 165 min (I=0.1 nA V=3 V); c) after UHV heating to 500° C for 330 min (I=0.1 nA V=3 V) the green arrows indicate regions in which the clusters are preferentially located on step edges; d) same as c, but with different bias (I=0.08 A V=-1.4 V).

surface reduction. A further thermal treatment for the same time (165 min) at the same temperature (500°C) gives rise to a non negligible degree of reduction as measured by XPS ($c_{Ce3+}=15\%$, spectrum not shown). The morphology (Fig.6c) shows the appearance of protrusions, similar in size and shape to the ones observed in Fig.4e and 5c and d, although with a lower density. A closer inspection shows a slight tendency for the protrusions to be preferentially located at the step edges of the cerium oxide features, as indicated by the green arrows in Fig.6c. The long range morphology of the 10 ML film is not altered by the thermal treatment.

The origin of the observed features is discussed in section 4.

3.3 LEED

To investigate possible modifications of the surface long range order after reduction, we measured the LEED patterns of the 2 and 10 ML samples at different reduction degrees. The LEED pattern of the 2 ML film after preparation (Fig.7a) shows the superposition of two hexagonal patterns, one related to the partially uncovered Pt surface (outer spots) and one related to the $CeO_2(111)$ film surface (inner spots). The sharpness and the geometry of the spots coming from the ceria film confirm the good crystal quality and epitaxy of cerium oxide on Pt in spite of the large lattice mismatch, as already observed for cerium oxide films on a number of different substrates. 7,10-13 No moiré pattern is observed, probably due to the fact that the cerium oxide structures have a minimum thickness of 2 ML. At intermediate reduction degrees the LEED pattern shows the appearance of a reconstruction around the ceria-related spots. An example is shown in Fig.7b, which reports the LEED pattern of the 2 ML sample after a thermal treatment in UHV at 500°C for 30 min, which leads to a Ce³⁺ concentration of 40% as measured by XPS. It consists of a (3×3) periodicity with respect to the cerium oxide surface cell with extra spots between superstructure spots. An inspection of the position of the extra spots shows that they do not lie on the line which joins two (3x3)-related spots, being closer to the (1×1) ceria spots and ascribed to a $9/4(\sqrt{3}\times\sqrt{3})R30^{\circ}$ periodicity. If the film is further reduced, i.e. for Ce3+ concentration between 60% and 80%, the (3×3) periodicity disappears and only the $9/4(\sqrt{3}\times\sqrt{3})R30^{\circ}$ periodicity is left, as shown in Fig.7c which corresponds to a sample heated at 770°C for 15 min.

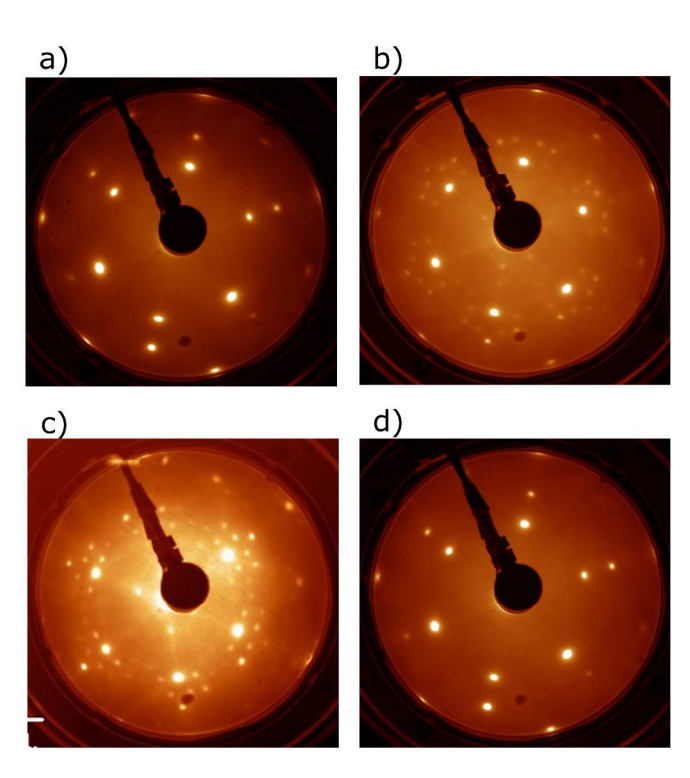


Fig. 7: LEED patterns (Ep=80 eV) of a 2 ML cerium oxide film a) as prepared, b) after intermediate reduction by heating in UHV at 500°C for 30 min ($c_{\text{Ce3+}}$ ~40%), showing the (3×3) and the 9/4($\sqrt{3}\times\sqrt{3}$)R30°phase c) after strong reduction by heating in UHV at 770°C for 15 min ($c_{\text{Ce3+}}$ ~60-80%) showing the 9/4 ($\sqrt{3}\times\sqrt{3}$)R30° phase d) after re-oxidation by heating in O₂ at 770 °C.

Whatever the degree of reduction, the surface structure can always be brought back to the original one after a thermal treatment in O_2 at 770° C for 15 min, as shown in Fig.7e.

The LEED pattern of the 10 ML film after preparation shows only the CeO_2 -related spots (Fig.8a), since the substrate coverage is complete. After reduction only a signal-to-background decrease is observed (Fig.8b), indicating some degree of surface disorder. The original surface structure also in this case is restored after the thermal treatment in O_2 , as shown in Fig.8c.

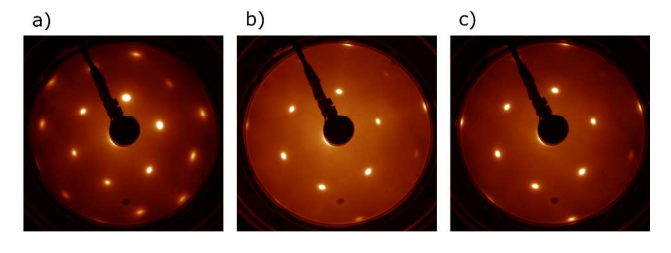


Fig.8: LEED patterns (Ep=80 eV) of a 10 ML cerium oxide film a) as prepared, b) after UHV heating at at 770° C and c) after re-oxidation by heating in O₂ at 770° C.

4. Discussion

XPS results indicate that cerium oxide films can reduced by thermal treatments in UHV and reoxidized by thermal

treatments in O_2 , obtaining the desired Ce^{3+} concentration within a continuous range. At the highest temperatures used in the present study (770°C to avoid intermixing with the substrate) the reduction is not complete (Fig.3). This evidence is not surprising and it can be ascribed to the limited heating temperature, which does not induce a large enough mobility to the oxygen atoms in the inner layers.

The difference in the maximum Ce³⁺ concentration measured for the 2 and 10 ML samples (Fig.3c and d) is not by itself an evidence for a different absolute concentration of surface oxygen vacancies in the two samples. In fact, it can be partly due to the fact that reduction occurs mainly in the topmost layers (cfr Fig.2) and to the limited probing depth of the XPS technique. Following Tanuma et al., 41 an inelastic mean free path of 13 Å for Ce 3d photoelectrons was estimated. This value is larger than the thickness of the nominally 2 ML film (also taking into account the actual morphology, see section 3.2) and significantly smaller than the thickness of the 10 ML sample. The estimate of an absolute value of surface concentration of Ce³⁺ is hindered by the fact that the depth profile of the Ce³⁺ concentration in the sample is unknown. Therefore we cannot exclude that the different values of Ce³⁺ concentration measured on thinner and thicker films actually reflect a comparable maximum degree of reduction.

The surface sensitivity of the XPS technique and the limited mobility of the oxygen ions from the inner layers at the considered temperature may also explain the higher degree of reduction measured in this study compared to the one measured for thicker films on Si in different studies.¹⁵

The temperature at which reduction starts is lower for the 2 ML (200°C) than for the 10 ML film (450°C). A lower oxygen vacancy formation energy is expected for undercoordinated oxygen atoms at steps and kinks. 42 However, the STM images show that the surface density of steps and defects is comparable in 2 ML films, formed by cerium oxide islands which protrude from the Pt surface, and in 10 ML films, which also show an irregular surface morphology with small ceria islands on top of cerium oxide layers with holes exposing the underlying oxide planes (Fig.4 a and d). The oxygen vacancy formation energy was predicted to be much smaller in systems of nanometric size than in extended surfaces, even at step edges. 42 This effect may come into play in the 2 ML film, where the vertical and lateral size are limited to approximately 1 nm and a few tens of nm, respectively. Another possible reason for the observed decrease in the onset temperature for reduction in the 2 ML film is the proximity of the Pt substrate, which is expected to transfer some charge to the oxide³⁹ and may alter the oxygen vacancy formation energy at low temperatures.

The temperature necessary for reoxidation is higher in the 2 ML sample than on the 10 ML one, consistent with a lower stability of the oxidized phase in the thinner films due to charge transfer from Pt. The non complete oxidation of the 10 ML sample at low temperature may be due to a high density of vacancies in subsurface sites also in heavily reduced surfaces²⁰ and to the limited mobility of oxygen ions at low temperature.

A substrate-induced difference in the surface structure of the reduced phases is observed also in the LEED patterns of the 2 and 10 ML films after the thermal treatments (Fig.7b,c and Fig.8b). The presence of the Pt substrate probably influences the oxygen vacancy formation energy in the 2 ML film, in particular by modulating it within the coincidence cell and leading to the stabilization of new bidimensional oxide phases with ordered surface oxygen vacancies. To understand the origin of the superstructures observed in LEED for the 2 ML film after reduction (Fig.7b and c), the dominant epitaxial

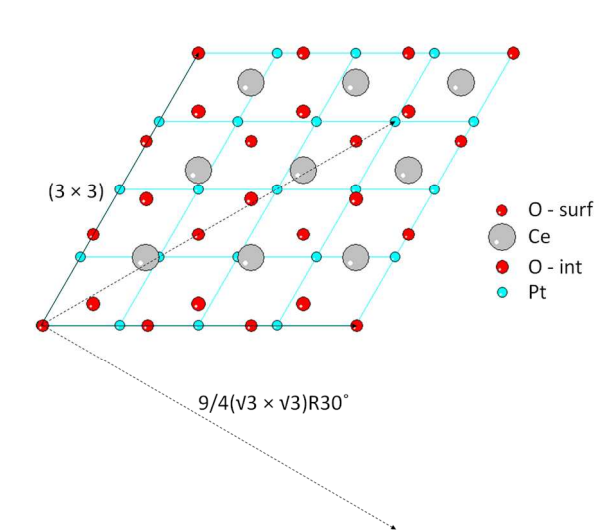


Fig. 9: Model of the 3:4 coincidence cell at the interface between CeO_2 and Pt(111). Four Pt surface unit cells (Pt atoms are represented as light blue spheres) coincide with three CeO_2 surface unit cells (interface O atoms are represented as large red spheres, Ce atoms as grey spheres and surface O atoms as small red spheres). The (3×3) supercell (solid line)and the $9/4(\sqrt{3}\times\sqrt{3})R30^\circ$ supercell (dashed lines) are also shown.

relation between cerium oxide films and Pt has to be considered. The cerium oxide surface lattice parameter in thin films is slightly contracted to have a $3a_{CeO_2}=4a_{Pt}$ coincidence. 6,10,43 The film/substrate coincidence cell is therefore three times larger than the surface cell of the cerium oxide film (Fig.9). The observed (3×3) periodicity might be caused by a substrate-induced height modulation of the film, due to the larger in-plane interatomic distance of the reduced phase, with some regions being more strongly bound to the surface in the different sites of the coincidence cell. This hypothesis however seems rather unlikely due to the fact that the minimum thickness of the film is 2 ML and the reduction mainly occurs at the surface. Alternatively, the (3×3) periodicity may be due to the preferential formation of oxygen vacancies in specific sites of the coincidence cell, which could be induced by a local modulation of the oxygen vacancy formation energy, caused by the different adsorption geometries of the film atoms with respect to the substrate within the coincidence cell. As shown in Fig.9 also the $9/4(\sqrt{3}\times\sqrt{3})R30^{\circ}$ periodicity coincides with specific Pt atoms. Spiel et al. have calculated that in a 1 ML cerium oxide film on Pt(111) the interatomic distances and the charge transfer are locally modulated within the coincidence cell.³⁹ These effects are expected to induce local variations also of the oxygen vacancy formation energy. The formation of ordered arrays of oxygen vacancies on the surface of ultrathin cerium oxide layers was already observed on other substrates. 11,30,33 For the cerium oxide films investigated in the present work, however, it is not straightforward to establish a direct correlation between the surface superstructure and the Ce³⁺ concentration. The $9/4(\sqrt{3}\times\sqrt{3})$ R30° periodicity is larger than the (3×3) periodicity, while the Ce³⁺ concentration is higher for the $9/4(\sqrt{3}\times\sqrt{3})R30^\circ$ phase. The different degree of reduction can be explained by different oxygen vacancies concentration formed in the inner layers. The observed reduced cerium oxide phases have a lower oxygen vacancy concentration than the c-Ce₂O₃ phase, which

gives a (4×4) superstructure on the cerium oxide surface,³³ never observed in the present study. The a-Ce₂O₃(0001) surface instead would give a hexagonal diffraction pattern, less than 2% contracted with respect to the CeO₂(111) one, very hard to be resolved experimentally. A more complete understanding of the observed phases indeed requires a three dimensional structural characterization.

The possible presence of surface height modulations or of surface superstructures was checked by STM. The expected periodicity is 1.1 nm for the (3×3) reconstruction and 1.5 nm for the $9/4(\sqrt{3}\times\sqrt{3})R30^\circ$. The apparent protrusions in the STM images of the reduced samples are a few nm wide and their presence probably hinders the possibility of directly observing either ordered superstructures and/or a height modulation. The absence of any surface reconstruction in thicker films after reduction (Fig.8b) is due to the lack of preferential sites for oxygen vacancy formation in thick films, where the substrate proximity effects are much less effective. In this case oxygen loss proceeds randomly and gives rise to the observed signal-to-background decrease.

The bright features observed in the STM images after reduction (Fig.4b and e, Fig.5b and Fig.6c) can originate from agglomerations of reduced ceria, which – having a larger lattice parameter – protrude from the surface in small clusters. The tendency for oxygen vacancies to aggregate or repel is still a matter of debate.²⁰ A separation between reduced and non reduced areas might be induced by some O vacancy agglomeration. 44 In this hypothesis we cannot exclude that the reduced material in the protrusion forms the edge structure after reoxidation (Fig.5c). It is more likely, however, that the observed protrusions are apparent and due to local modifications of the empty states after significant reduction. A decrease of the band gap of cerium oxide films after reduction, due to the filling of 4f states in the gap, and a modification of the empty conduction band of the material have been measured.²³ Large bright protrusions in the STM, similar to the ones observed in this study, were measured also on MgO film surfaces and assigned to surface color centers, based on their bias dependence. In a recent study by the same group ceria surface defects were studied by scanning tunneling spectroscopy. 46 The empty conduction band was shown to be shifted to lower biases at specific defect sites corresponding to oxygen vacancies. The small features observed in this study, rather than being real protrusions, could be connected with the presence of reduced cerium sites on the surface and to the consequent local modifications of the empty conduction band after extensive reduction. The images shown in Fig.6a,b,c are acquired at a positive sample bias of 3 V, i.e. probing the empty states of ceria. Good quality images at positive sample biases much smaller than 3 V have a much lower quality. Fig.6d is an image of the same sample, acquired at a negative sample bias of -1.4 V and it shows no protrusions on the surface. This allows to preferentially assign the observed features to electronic effects rather than to real protrusions. Of course, a conclusive statement on the origin of the observed features requires a measurement and/or a calculation of the empty states band structure also on a heavily reduced ceria surface.

5. Conclusions

Epitaxial cerium oxide films on Pt(111) are significantly reduced by thermal treatments in UHV. The reduction occurs mainly at the surface but it extends partly also to subsurface layers. The maximum Ce³⁺ concentration obtained at

Journal Name ARTICLE

intermediate temperatures depends on film thickness, due to the influence of the Pt substrate, which modifies the energy for oxygen vacancy formation. The Ce³⁺ concentration also strongly depends on the heating rate and heating time, showing that the formation of oxygen vacancies on the surface and the thermally activated oxygen diffusion from inner layers reach an equilibrium at each given temperature within times of the order of hours. The surface morphology shows apparent protrusions after significant reduction, which are possibly due to local modifications of the cerium 5d band with reduction. The formation of reduced cerium oxide phases with ordered surface superstructures is observed only for thin films and it is ascribed to the proximity of the Pt substrate, which spatially modulates the oxygen vacancy formation energy. Reduced phases with (3×3) and $9/4(\sqrt{3}\times\sqrt{3})R30^{\circ}$ surface superstructure were observed at different degrees of reduction. The film stoichiometry, morphology and surface structure can be brought back to the original one after thermal treatments in oxygen.

Acknowledgements

The work was supported by the Italian MIUR through the FIRB Project RBAP115AYN "Oxides at the nanoscale: multifunctionality and applications" and by the COST Action CM1104 "Reducible oxide chemistry, structure and functions".

References

- A. Trovarelli, P. Fornasiero. Catalysis by Ceria and Related Materials. London: Imperial College Press, 2013.
- H. L. Tuller, S. J. Litzelman and W. C. Jung, *Phys. Chem. Chem. Phys.* 2009, 11, 3023.
- 3 I. Celardo, J. Z. Pedersen, E. Traversa and L. Ghibelli, *Nanoscale*. 2011, **3**, 1411.
- 4 F. Esch, S. Fabris, L. Zhou, T. Montini, C. Africh, P. Fornasiero, G. Comelli and R. Rosei, *Science*, 2005, **309**, 752.
- 5 J.-F. Jerratsch, X. Shao, N. Nilius, H.-J. Freund, C. Popa, M. V. Ganduglia-Pirovano, A. M. Burow and J. Sauer, *Phys. Rev. Lett.* 2011, 106, 246801.
- 6 C. Hardacre, G. M. Roe and R. M. Lambert, Surf. Sci., 1995, 326, 1.
- 7 K.-D. Schierbaum, Surf. Sci., 1998, 399, 29.
- 8 K.-D. Schierbaum and U. Berner, Phys. Rev. B, 2002, 65, 235404.
- D. C. Grinter, R. Ithnin, C. L. Pang and G. Thornton, J. Phys. Chem C, 2010, 114, 17036.
- P. Luches, F. Pagliuca and S. Valeri, J. Phys. Chem. C, 2011, 115, 10718
- S. Eck, C. Castellarin-Cudia, S. Surnev, M.G. Ramsey and F.P. Netzer. Surf. Sci., 2002, 520, 173.
- J.-L. Lu, H.-J. Gao, S. Shaikutdinov and H.-J. Freund, Surf. Sci., 2006, 600, 5004.
- 13. T. Staudt, Y. Lykhach, L. Hammer, M. A. Schneider, V. Matolín and J. Libuda. *Surf. Sci.*, 2009, **603**, 3382.
- J. I. Flege, B. Kaemena, S. Gevers, F. Bertram, T. Wilkens, D. Bruns and J. Batjer, *Phys. Rev. B*, 2011, **84**, 235418.
- H. Wilkens, O. Schuckmann, R. Oelke, S. Gevers, M. Reichling, A. Schaefer, M. Bäumer, M. H. Zoellner, G. Niu, T. Schroeder and J. Wollschläger. *Phys. Chem. Chem. Phys.*, 2013, 15, 18589.

- S. Tobrügge, M. Cranney and M. Reichling, Appl. Phys. Lett., 2008, 93, 073112.
- 17. H. Nörenberg and G. A. D. Briggs, Phys. Rev. Lett., 1997, 79, 4222.
- C. Castellarin-Cudia, S. Surnev, G. Schneider, R. Podlucky, M.G. Ramsey and F. Netzer, Surf. Sci., 2004, 554, L120.
- M. V. Ganduglia-Pirovano, J. L. F. Da Silva and J. Sauer, *Phys. Rev. Lett.*, 2009, 102, 4.
- G. E. Murgida and M. V. Ganduglia-Pirovano, *Phys. Rev. Lett.*, 2013, 110, 246101.
- S. Tobrügge, M. Reichling, A. Ishiyama, S. Morita and O. Custance, *Phys. Rev. Lett.*, 2007, 99, 056101.
- F. Dvořák, O. Stetsovych, M. Steger, E. Cherradi, I. Matolínová, N. Tsud, M. Škoda, T. Skála, J. Mysliveček and V. Matolín, *J. Phys. Chem. C*, 2011, 115, 7496.
- 23. A. Pfau and K. D. Schierbaum. Surf. Sci., 1994, 321, 71.
- S. D. Senanayake, D. Stacchiola, J. Evans, M. Estrella, L. Barrio, M. Pérez, J. Hrbek and J. A. Rodriguez. *J. Catal.* 2010, Vol. 271, p. 392.
- V. Matolín, J. Libra, M. Škoda, N. Tsud, K.C. Prince and T. Skála. Surf. Sci., 2009, 603, 1087.
- D.R. Mullins, S.H. Overbury and D.R. Huntley, Surf. Sci., 1998, 409, 307.
- E. L. Wilson, Q. Chen, W. A. Brown and G. Thornton, *J. Phys. Chem C*, 2007, 111, 14215.
- D. R. Mullins, P. V. Radulovic and S. H. Overbury, Surf. Sci., 1999, 429, 186.
- B. Kaemena, S. D. Senanayake, A. Meyer, J. T. Sadowski, J. Falta and J. I. Flege, *J. Phys. Chem C*, 2013, 117, 221.
- H. Wilkens, O. Schuckmann, R. Oelke, S. Gevers, A. Schaefer, M. Bäumer, M. H. Zoellner, T. Schroeder and J. Wollschläger. *Appl. Phys. Lett.*, 2013, 102, 111602.
- 31. W. Xiao, Q. Guo and E. G. Wang, Chem. Phys. Lett., 2003, 368, 527.
- 32. J. I. Flege, B. Kaemena, S. Gevers, F. Bertram, T. Wilkens, D. Bruns, J. Batjer, T. Schmidt, J. Wollschlager and J. Falta, *Phys. Rev. B*, 2011, **84**, 235418.
- 33. V. Stetsovych, F. Pagliuca, F. Dvořák, T. Duchoň, M. Vorokhta, M. Aulická, J. Lachnitt, S. Schernich, I. Matolínová, K. Veltruská, T. Skála, D. Mazur, J. Mysliveček, J. Libuda and V. Matolín, *J. Phys. Chem. Lett.*, 2013, 4, 866.
- M. Romeo, K. Bak, J. El Fallah, F. Le Normand and L. Hilaire. Surf. Interface Anal. 1993, 20, 508.
- 35. T. Skála, F. Šutara, M. Škoda, K. C. Prince and V. Matolín. *J. Phys: Condens. Matter.*, 2009, 21, 055005.
- 36. P. Burroughs, A. Hamnett, A. F. Orchard and G. Thornton, *J. Chem. Soc. Dalton Trans.*, 1976, 1686.
- 37. A. Kotani and H. Ogasawara, J. El. Spec. Rel. Phen., 1997, 86, 65.
- I. Horcas, R. Fernández, J. M. Gómez-Rodríguez, J. Colchero, J. Gómez-Herrero and A. M. Baro, Rev. Sci. Instrum., 2007, 78, 013705.
- 39. C. Spiel, P. Blaha, Y. Suchorski, K. Schwarz and G. Rupprechter, *Phys. Rev. B*, 2011, **84**, 045412.
- 40. F. Pagliuca, P. Luches and S. Valeri, Surface Science, 2013, 607, 164.
- 41. S. Tanuma, C.J. Powell and D.R. Penn, Surf. Int. Anal., 1975, 25, 25.
- 42. A. Migani, G. N. Vayssilov, S. T. Bromley, F. Illas and K. M. Neyman, *J. Mater. Chem.*, 2010, **20**, 10535.
- P. Luches, F. Pagliuca, S. Valeri and F. Boscherini, *J. Phys. Chem. C*, 2013, 117, 1030.

Journal Name

44. J. C. Conesa, Surf. Sci. 1995, 339, 337.

- 45. M. Sterrer, M. Heyde, M. Novicki, N. Nilius, T. Risse, H.-P. Rust, G. Pacchioni and H.-J. Freund. *J. Phys. Chem. B*, 2006, **110**, 46.
- 46. X. Shao, J.-F. Jerratsch, N. Nilius and H.-J. Freund, *Phys. Chem. Chem. Phys.*, 2011, **13**, 12646.